Journal of the Iranian Chemical Society
https://doi.org/10.1007/s13738-021-02170-7

ORIGINAL PAPER

Nanomagnetic catalysis (Fe_3O_4@S–TiO_2): a novel magnetically nano catalyst for the synthesis of new highly substituted tetrahydropyridine derivatives under solvent-free conditions

Zahra Nezami[1] · **Hossein Eshghi**[1]

Received: 26 August 2020 / Accepted: 2 January 2021

Abstract

A novel nanomagnetic catalyst (Fe_3O_4@S–TiO_2) was prepared by the hydrothermal method. At the first, Fe_3O_4 nanoparticles were synthesized, then iron oxide nanoparticles (IONPs) were dispersed in ethanol solution, followed by the addition of titanium isopropoxide and thiourea to modify IONPs. The synthesized magnetically green catalyst has been characterized by various methods (TEM, SEM, EDS, XRD, VSM and FTIR). These techniques approved that the sulfur–doped titanium dioxide shell was well placed on the surface of the magnetite core. The catalytic activity of this nanocatalyst has been studied in the diastereoselective synthesis of new highly substituted tetrahydropyridine derivatives at 100 °C and under solvent-free conditions. It was confirmed that this nanocatalyst can multiply the rate of the reaction compared to the undoped Fe_3O_4@TiO_2 and can also lead to high reaction yields. This catalyst could be easily recovered and reused without significant loss of activity over five successful runs. Besides, we proved that acetylacetone can be an acceptable and effective β-diketone in the synthesis of tetrahydropyridines in high yields.

Graphic abstract

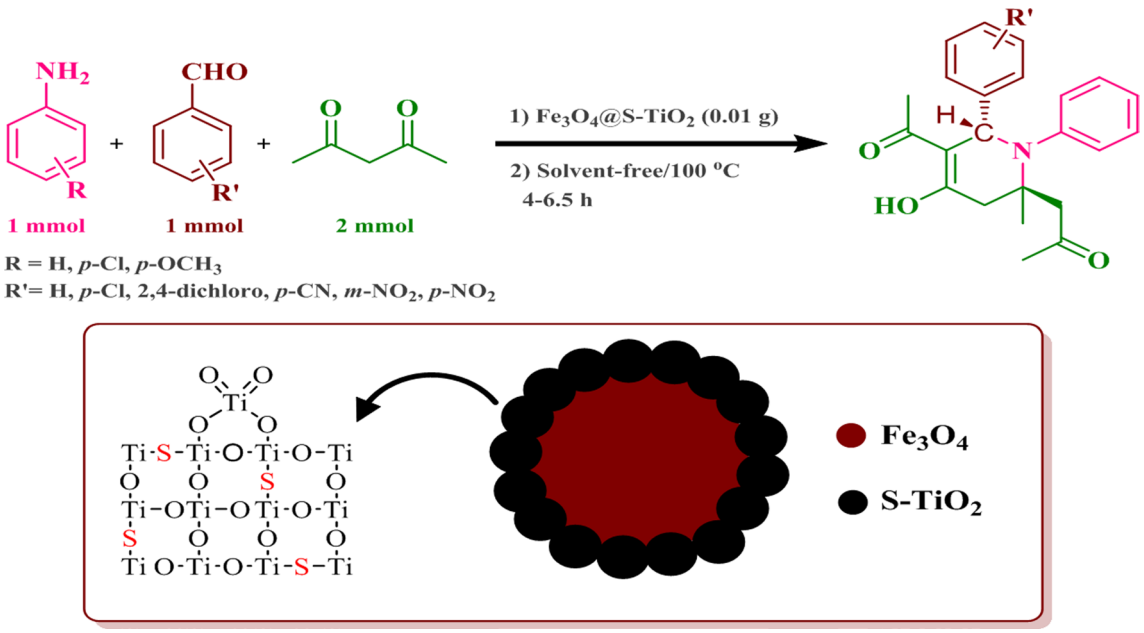

Supplementary Information The online version contains supplementary material available at https://doi.org/10.1007/s13738-021-02170-7.

Extended author information available on the last page of the article

Published online: 13 January 2021

Keywords Diastereoselective · Iron oxide nanoparticles · Nanomagnetic catalyst · Tetrahydropyridine

Introduction

Catalysis is a phenomenon that a substance (the catalyst) increases the rate of a chemical reaction without consuming in the process. Heterogeneous catalysis which includes a solid catalyst and gas- or liquid-phase reactants, is the most catalytic process in nature. When compared to homogeneous catalysts, heterogeneous catalysts present essential advantages not only because of their easy preparation, separation from the reaction mixture, ability to recycle but also due to their stability, low toxicity and low cost [1].

Recently, magnetic nanoparticles (MNPs) have received much attention because of their broad applications in different fields such as catalysis [2], biomedicine [3], etc. Iron oxide nanoparticles (IONPs) are the most popular among various types of MNPs due to their ease of surface modification, synthesis and recyclability [4]. The coating method is the most popular surface modification approach to place the organic or inorganic materials on the surface of IONPs. This method prevents the oxidation and agglomeration of IONPs, it also provides the possibility for further functionalization which improves their physicochemical properties [5].

Composite core–shell nanoparticles based on magnetic and semiconductor materials have been evoked great interest among scientists. TiO_2 nanocomposites have been widely studied due to their strong chemical and photochemical stability, low cost and nontoxicity [6–8]. Modifying the magnetic nanoparticles with TiO_2, not only protects the core against environmental damaging but also make the particles stable, desired functional and biocompatible [9]. Besides, these nanocomposites can have a convenient separation and recovery from the reaction mixture by using an external magnetic field [10]. Heteroatom doping of the Fe_3O_4@TiO_2 nanocatalyst can improve its catalytic activity. Non-metal dopants such as Sulfur (S) [11–14] have been used in many studies to modify the TiO_2 surface. It was reported to be beneficial for developing highly efficient TiO_2 that can have a significant role in the synthesis of organic compounds. The substitution of sulfur in either cationic or anionic sites depends on both the experimental conditions and the choice of precursor [15].

Multicomponent reactions (MCRs) have an important role in combinatorial chemistry because of their ability to generate many chemical compounds with more efficiency and atomic economy [16–21]. MCRs can synthesis the desired product in a single operation from three or more reactants molecules without exposure of toxic intermediate to the environment [22].

In recent years, compounds containing tetrahydropyridine (THPD) structures were used in biological characteristics as well as medicinal activities such as antimicrobial [23, 24], anti-influenza [25], antihypertensive [26], antibacterial [27], anticancer [28], anti-inflammatory activities [29], etc. Synthesis of THPDs using multicomponent reactions in the presence of different catalytic systems (e.g., L-proline, CAN, $Al(H_2PO_4)_3$) and many more have been performed [30–35].

In this study for the first time, we functionalized Fe_3O_4 MNPs with sulfur–doped TiO_2 (Fe_3O_4@S–TiO_2). This novel nanomagnetic recoverable catalyst was characterized with several techniques and finally, its catalytic performance was tested in the synthesis of new tetrahydropyridine derivatives at 100 °C and under solvent-free conditions. To the best of our knowledge, there are no examples of the use of heteroatom-doped core–shell nanocatalyst for the diastereoselective synthesis of THPDs derivatives from the condensation of aromatic amines, aromatic aldehydes and acetylacetone. Therefore, we reported an efficient and green synthetic method to synthesis these products using Fe_3O_4@S–TiO_2 as a heterogeneous novel catalyst.

Results and discussion

Magnetic iron oxide nanoparticles have been studied widely due to their applications such as their ease of surface modification, synthesis, low toxicity, recyclability, insoluble nature and magnetic properties. Major purposes of surface modification of magnetic iron oxide nanoparticles (IONPs) are to improve or change the dispersion of MNPs and the surface activity of MNPs. Surface coating with inorganic materials is one of the main procedures to synthesize magnetic iron oxide nanocomposites. Among the materials used in surface modification of magnetic nanoparticles, titanium dioxide (TiO_2) is one of the most important agents because of its high chemical stability, large effective surface area, easy availability and nontoxicity. Use of heteroatoms such as sulfur in design and synthesis of heteroatom-doped catalytic systems have a synergistic effect on catalytic activity. Heteroatom increases the electron density of catalyst, so surface adsorption of nanocatalyst increases. It results in a more effective and higher catalytic activity.

In this project, the major question in the design of the catalyst is that: can heteroatom doping of the catalyst increase reactivity and lead the reaction to a specific product with high efficiency?

Characterization of Fe_3O_4@S–TiO_2 NPs

The Fe_3O_4@S–TiO_2 was prepared by the concise method shown in Scheme 1. Naked magnetite nanoparticles were

Scheme 1 Preparation of Fe_3O_4@S–TiO_2

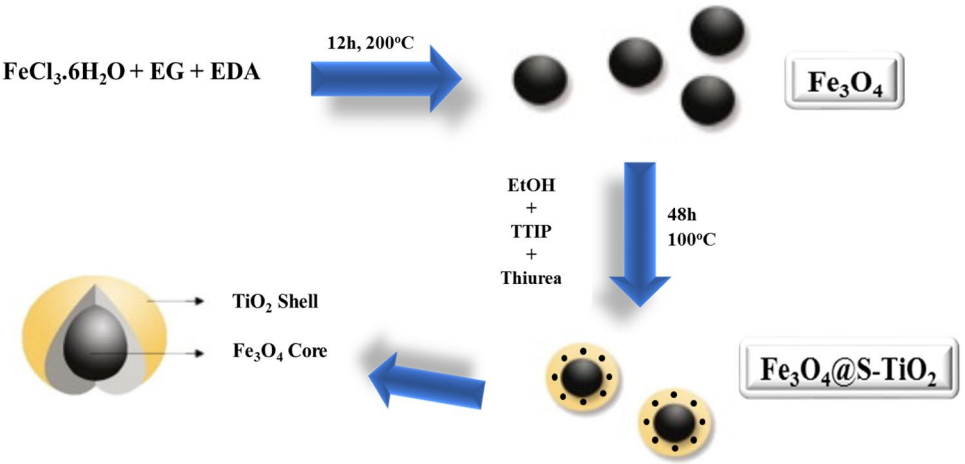

prepared via a hydrothermal treatment, and subsequently modified by titanium isopropoxide and thiourea to achieve Fe_3O_4@S–TiO_2 nanoparticles.

The catalyst has been characterized by various techniques including TEM, SEM, EDX (Fig. 1), XRD (Fig. 2), VSM (Fig. 3) and FTIR (Fig. 4). For the morphology study of the Fe_3O_4@S–TiO_2 MNPs, TEM and SEM were used (Fig. 1). The Fe_3O_4 MNPs are cuboid particles with an average diameter of about 60 nm (Fig. 1a). As shown in Fig. 1b, compared with Fig. 1a, the Fe_3O_4@S–TiO_2 show a Fe_3O_4 MNPs core within a shell that elemental analysis (Fig. 1g) also approves this elemental composition. The average shell thickness is about 20 nm, and the average diameter of the titanium dioxide nanoparticles is about 11 nm (Fig. 1b). SEM images of the catalyst show aggregation of the nanoparticles which can be due to the magnetic nature of them (Fig. 1c, d). TEM and SEM images of the recycled catalyst (Fig. 1e, f) did not show significant changes in morphology, also aggregation of the nanoparticles due to its magnetic nature has been maintained. The energy-dispersive X-ray spectroscopy (EDX) result shown in Fig. 1g demonstrates that the elements of the as-prepared nanocatalyst are Fe, O, Ti and S, and the

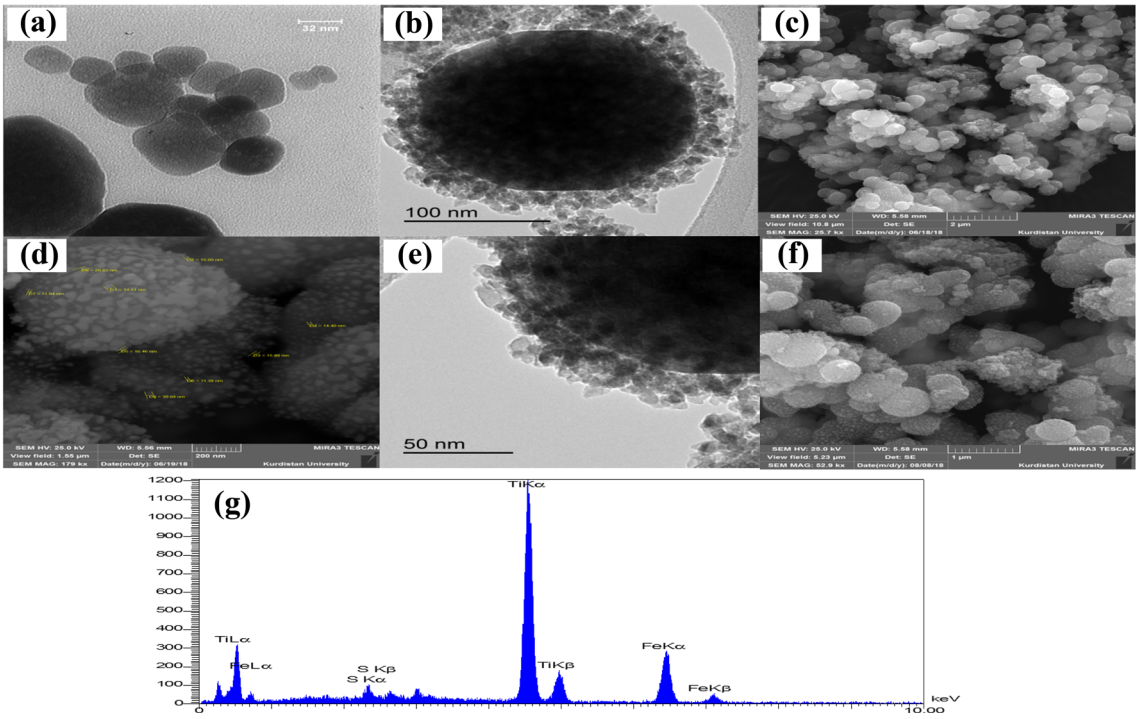

Fig. 1 TEM images of Fe_3O_4 and Fe_3O_4@S–TiO_2 (**a**, **b**) and SEM images of Fe_3O_4@S–TiO_2 (**c**, **d**), TEM and SEM images of recycled Fe_3O_4@S–TiO_2 (**e**, **f**), EDX image of Fe_3O_4@S–TiO_2 MNPs (**g**)

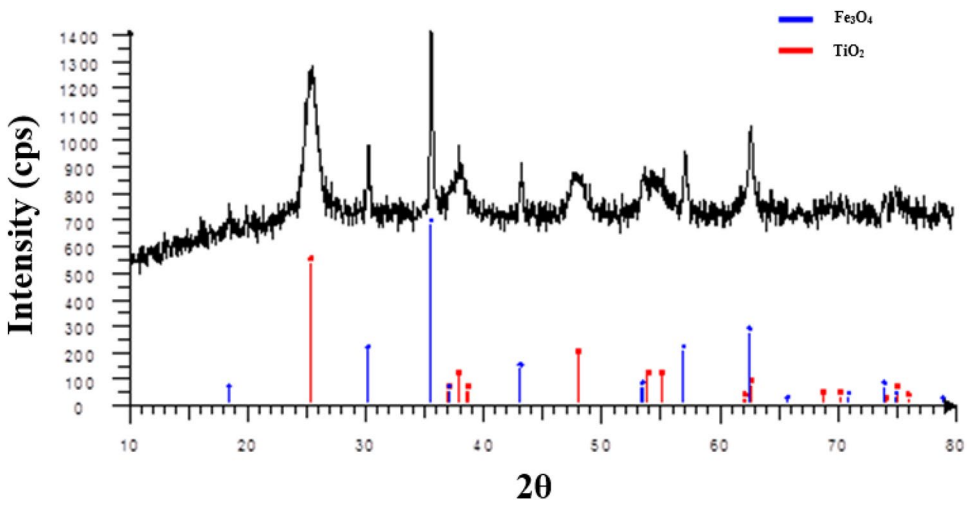

Fig. 2 XRD patterns of prepared Fe_3O_4@S–TiO_2

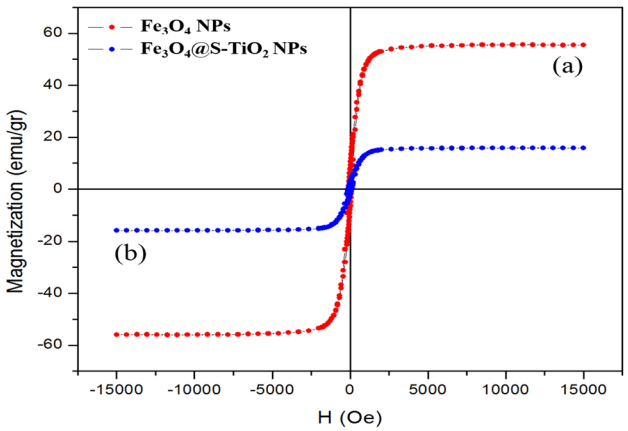

Fig. 3 VSM curves of prepared Fe_3O_4@S–TiO_2

catalyst is composed of Fe_3O_4, TiO_2 and S which agrees well with the EDX analysis. According to the quantitative results of EDX, mass percentage (W%) of Fe_3O_4, TiO_2 and also S are obtained 48.09, 51.28 and 0.63, respectively.

The phase purity of the Fe_3O_4@S–TiO_2 was investigated using XRD, as shown in Fig. 2. According to the JCPDS card no. 19-0629, twelve diffraction peaks appearing as blue lines located at 18.4, 30.1°, 35.5°, 37.1°, 43.1°, 53.4°, 57.0°, 62.6°, 70.8°, 74.0°, 75.0° and 79.0° can be assigned to diffraction of the Fe_3O_4 crystal with an inverse spinel structure from the (111), (220), (311), (222), (400), (422), (511), (440), (620), (533), (622) and (444) crystal planes. These results show that the phase of Fe_3O_4 MNPs has no change after the coating process. According to calculations with the Debye–Scherrer equation ($D = 0.9\lambda/\beta$

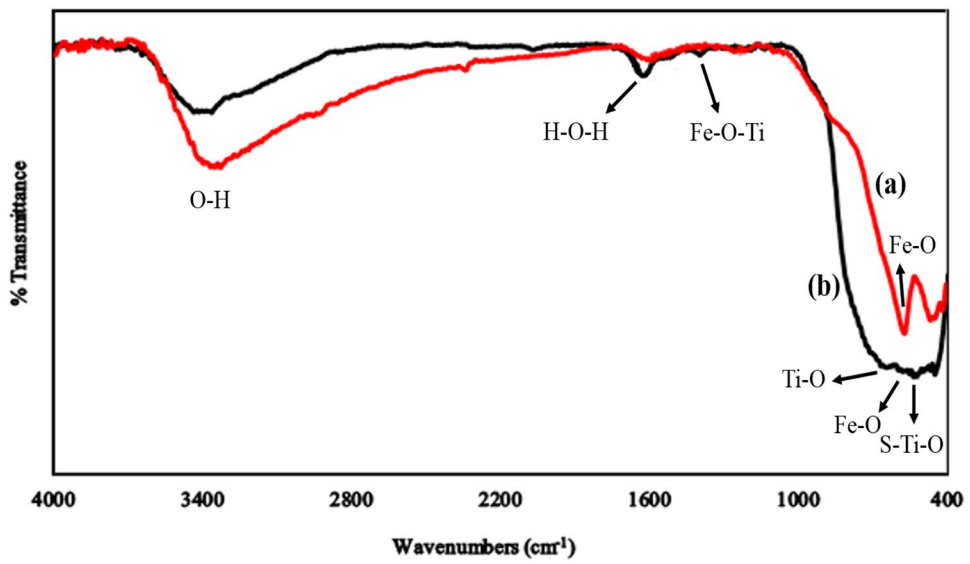

Fig. 4 FTIR spectra of **a** Fe_3O_4 and **b** Fe_3O_4@S–TiO_2

cos θ) for the five-strong peaks (220, 311, 400, 511 and 440), the average grain size of 26.2 nm for the Fe_3O_4 nanoparticles was measured. Also, according to the JCPDS card no. 21-1272 characteristic peaks were observed in the XRD pattern at 2θ of 25.3°, 37.0°, 37.9°, 38.6°, 48.0°, 54.0°, 55.0°, 62.1°, 62.8°, 68.8°, 70.3°, 74.0°, 75.0° and 76.0° shown as red lines in Fig. 2 correlate with the (101), (103), (004), (112), (200), (105), (211), (213), (204), (116), (220), (107), (215) and (301) crystal faces of TiO_2 tetragonal structure. Peak broadening was indicating the small size of nanoparticles. The crystallite size of nanoparticles was evaluated from the XRD data using Debye–Scherrer equation ($D = 0.9\lambda/\beta \cos\theta$). Average crystallite size for the three strong peaks (101, 004 and 200), was 7.78 nm for the TiO_2 nanoparticles.

The magnetic properties of Fe_3O_4 and Fe_3O_4@S–TiO_2 were investigated by VSM. The room temperature magnetization curves of Fe_3O_4 and Fe_3O_4@S–TiO_2 are shown in Fig. 3a, b in the applied magnetic field sweeping from − 15 to 15 kOe. The magnetic saturation (M_s) value of the Fe_3O_4 and Fe_3O_4@S–TiO_2 MNPs is 56.67 and 16.25 emu g^{-1}, respectively. Decrease of magnetic saturation value of iron ions connected to Ti by Fe–O–Ti bond has been reported before [36, 37]. Therefore, the decrease of M_s value due to the modification of magnetite core by titanium dioxide shell was expected. According to the previous studies [38], percent of magnetic saturation in Fe_3O_4/Fe_3O_4@TiO_2 reduced from 100 to 71 (average shell thickness about 10 nm) as well as 28% reduction in M_s value in this work. Due to the shell thickness (20 nm) and the presence of sulfur in the catalyst structure, a significant reduction in the magnetic saturation can be related to these two cases.

The FTIR spectra of Fe_3O_4 and Fe_3O_4@S–TiO_2 are compared in Fig. 4. The FTIR spectrum of uncoated Fe_3O_4 MNPs (Fig. 4a) shows a peak around 538 cm^{-1} due to the stretching of the Fe–O bond. The broad peak at 3358 cm^{-1} corresponds to the stretching vibrations of residual hydroxyl groups. The FTIR spectrum of Fe_3O_4@S–TiO_2 (Fig. 4b) shows a broad peak in the region around 500–700 cm^{-1} which can be the result of several peaks overlapping, correspond to the stretching vibrations of S–Ti–O, Fe–O and Ti–O in 534 cm^{-1}, 538 cm^{-1} and 649 cm^{-1}, respectively. The introduction of titanium isopropoxide to the surface of Fe_3O_4 is confirmed by the bands at 1397 cm^{-1} and 1621 cm^{-1} assigned to the Fe–O–Ti stretching vibration and O–H bending vibration, respectively. The broad peak at 3366 cm^{-1} implies the existence of hydroxyl groups on the surface of nanocatalyst. Decrease of the intensity of the broad peak in the 3300–3400 cm^{-1} range in comparison with spectrum 4a, is the result of the decrease of water molecules on the catalyst surface due to the hydrothermal process.

Synthesis of new tetrahydropyridines derivatives with Fe_3O_4@S–TiO_2 NPs

After the successful preparation and characterization of the Fe_3O_4@S–TiO_2 NPs, catalytic functioning of this nanocatalyst was investigated in the pseudo-four-component reaction of aromatic amines, aromatic aldehydes and acetylacetone.

In the beginning, to optimize the reaction conditions, the synthesis of compound **4g** in the presence of as-prepared catalyst was used as a model reaction. Therefore, in order to investigate the effect of solvent on the reaction product, a mixture of *p*-Cl aniline (1.0 mmol), *p*-Cl benzaldehyde (1.0 mmol), acetylacetone (2.0 mmol) and catalyst (0.01 g) was heated in different solvents and solvent-free conditions. After 5 h and due to the completion of the reaction, separation of catalyst and purification process was performed. As shown in Table 1, the yield and also purity of the reaction at 100 °C and under solvent-free conditions was greater than the other solvents (entry 10). Low yield and more impurity were the results of using non-polar solvents such as dichloromethane, dichloroethane and chloroform (entries 1–3). The yield of the reaction in the polar solvents such as acetonitrile and water was more than non-polar solvents (entries 4–7). These results showed that an increase in the reaction temperature leads to higher yields (according to the boiling point of the solvents). Reaction yield in acetic acid as a polar solvent was close to the solvent-free reaction, but according to the benefits of the green chemistry, solvent-free conditions was selected (entries 9 and 10).

Next, to find the optimum amount of Fe_3O_4@S–TiO_2, the reaction of *p*-Cl aniline, *p*-Cl benzaldehyde and acetylacetone were carried out under the previously mentioned conditions and at 100 °C using different amounts of catalyst (Table 2). The yield of the reaction in the absence of the catalyst (entry 1) resulted in the lowest value, showing that the catalyst has a significant effect on the reaction. Increasing

Table 1 Comparison of different solvents for synthesis of tetrahydropyridine (**4g**)

Entry	Solvent	Temperature (°C)	Time (h)	Yield (%)
1	CH_2Cl_2	40	6	5
2	$ClCH_2CH_2Cl$	83	6	35
3	$CHCl_3$	61	6.5	35
4	CH_3CN	82	5	50
5	MeOH	64	5	55
6	H_2O	100	5	60
7	EtOH	78	5	55
8	Toluene	110	5	50
9	CH_3COOH	118	4.5	90
10	**–**	**100**	**5**	**95**

Table 2 Comparison of the amount of Fe_3O_4@S–TiO_2 and Fe_3O_4@TiO_2, and yields for synthesis of tetrahydropyridine (**4g**)

Entry	Conditions	Catalyst	Catalyst amount (g)	Time (h)	Yield (%)
1	Solvent-free/100 °C	–	–	5	15
2	Solvent-free/100 °C	Fe_3O_4@S–TiO_2	0.005	5	75
3	**Solvent-free/100** °C	**Fe_3O_4@S–TiO_2**	**0.01**	**5**	**95**
4	Solvent-free/100 °C	Fe_3O_4@S–TiO_2	0.02	5	96
5	Solvent-free/100 °C	Fe_3O_4@TiO_2	0.01	48	96

the amount of the catalyst enhanced the yield of the product **4g** (entries 2 and 3). Using 0.01 g of the catalyst resulted in the highest yield in 5 h (entry 3). The higher amount of the catalyst did not increase the yield of the reaction considerably (entry 4). Furthermore, the model reaction was investigated in presence of a non-doped catalyst (Fe_3O_4@TiO_2), the reaction needed much more time to complete and had lower yield in same conditions in comparison to the doped catalyst (entry 5). This was exactly the result that we expected from the doped catalyst with a heteroatom. Heteroatom increased the electron density of catalyst, so reactants adsorption on its surface-enhanced and the result of this synergistic effect was multiplied the reaction rate by approximately 10 times.

Acetyl acetone is a β-diketone which has two tautomeric forms in equilibrium with each other. In the enol form, hydrogen atom is divided equally between the two oxygen atoms. This bifunctional compound is an effective precursor for the synthesis of heterocyclic compounds. Both keto groups in its structure can undergo condensation. Also, acidic protons between two carbonyl groups in the structure of acetylacetone make a strong proper nucleophile. In this study, our effort was to approve that acetylacetone is an effective β-diketone in the synthesis of new highly substituted tetrahydropyridines. Mannich reactions using β-ketosters (not acetylacetone) have been reported widely before [39], but high yields of the products using acetylacetone as a precursor have not been reported so far.

With the optimized reaction conditions in hand, the catalytic activity of this new catalyst was examined, and the results were summarized in Table 3. The corresponding compounds (4a–j) were synthesized by the reaction of amines, aldehydes and acetylacetone using 0.01 g of Fe_3O_4@S–TiO_2 at 100 °C and under solvent-free conditions (Scheme 2). 0.01 g (10 mg) of the catalyst which is used in each reaction equals to 6.4 mol% of the reactant according to the mass percentage of titanium dioxide. As shown in Table 3, we found that this domino cyclization reaction in the presence of nanomagnetic heteroatom-doped catalyst works well with a wide variety of substrates. In all the performed reactions, the anti-isomer was obtained exclusively. All selected aromatic amines and aldehydes such as electron-rich and electron-deficient aryl groups, reacted smoothly with acetylacetone to give the corresponding product in moderate to high yield. The presence of the nitro group in the para position of the benzaldehyde gave a higher yield of the product (entries 3 and 4). The electron-donating substituents in the aniline ring such as O–Me showed the same electronic effect as aniline ring (entries 5 and 10).

The reusability and recovery of the nanocatalyst were investigated in the optimized reaction conditions. At the

Table 3 Synthesis of tetrahydropyridine derivatives (**4a–j**) using of Fe_3O_4@S–TiO_2 as catalyst

Entry	*R*	*R′*	Product	Time (h)	Yield (%)[a]	M_p (°C)	TON	TOF[b] (h^{-1})
1	H	H	**4a**	5	88	89–90 (decompose)	13.75	2.75
2	H	*p*-Cl	**4b**	5	86	236–238	13.44	2.69
3	H	*m*-NO_2	**4c**	5	90	87–88 (decompose)	14.06	2.81
4	H	*p*-NO_2	**4d**	4	95	243–245	14.84	3.71
5	H	*p*-CN	**4e**	5.5	71	88–90 (decompose)	11.09	2.02
6	H	2,4$(Cl)_2$	**4f**	5.5	90	226–228	14.06	2.56
7	*p*-Cl	*p*-Cl	**4g**	5	95	238–240	14.84	2.97
8	*p*-Cl	*p*-NO_2	**4h**	5.5	82	84–85 (decompose)	12.81	2.33
9	*p*-OMe	*p*-NO_2	**4i**	6	79	213–215	12.34	2.06
10	*p*-OMe	*p*-CN	**4j**	5.5	78	88–90 (decompose)	12.19	2.21

Reaction Conditions: Aniline **1** (1.0 mmol), Benzaldehyde **2** (1.0 mmol), Acetylacetone **3** (2.0 mmol) and Fe_3O_4@S–TiO_2 (6.4 mol%) at 100 °C and under solvent-free conditions

[a]Isolated Yields

[b]TOF = TON/time (h) of the reaction, (TON = moles of product formed per mole catalyst)

Scheme 2 Synthesis of tetrahydropyridine derivatives in presence of Fe_3O_4@S–TiO_2

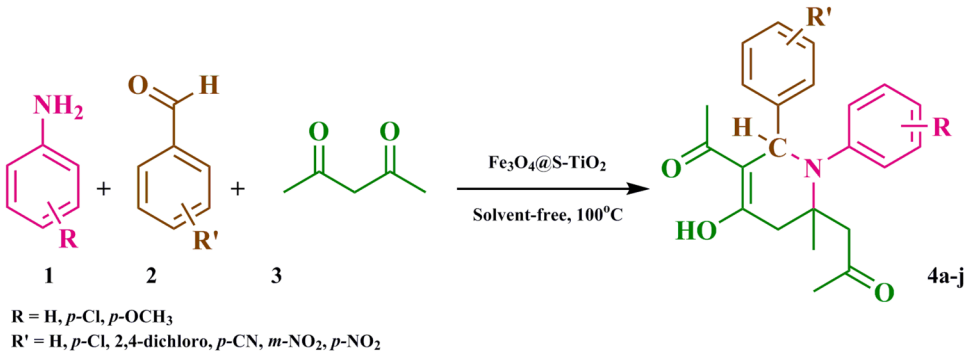

end of each reaction, hot acetone was added to the reaction mixture to dissolve the product, and the Fe_3O_4@S–TiO_2 was separated from the reaction mixture by employing an external magnetic field. The separated catalyst thoroughly washed with distilled water and ethanol for three times to remove the residual product and dried at 50 °C. Catalyst reused in the next reaction without considerable loss of its activity after five new runs (Fig. 5).

As shown in Scheme 3, the proposed mechanism was explained. This reaction was made up of two major parts in which two continuous Mannich reactions occur. It is reasonable to assume that the reaction between benzaldehyde and the amine leads to the formation of iminium ion firstly. Next, acetylacetone that its carbonyl group was activated with Fe_3O_4@S–TiO_2, proceeds to execute a nucleophilic attack on the imine. This attack yields the required β-amino carbonyl compound **A** (Intermolecular Mannich Reaction). Then, β-amino carbonyl **A** reacts with the second mole of acetylacetone. After producing two other intermediates and elimination of H_2O, an intramolecular Mannich reaction **B** takes place to give the desired tetrahydropyridine derivatives **C**.

As mentioned before, the catalyst that has been used in this reaction was a core–shell catalyst. The purpose of selecting a magnetic core (Fe_3O_4) was its ease of separation at the end of each reaction from the reaction mixture with the aid of an external magnetic field. Sulfur-doped TiO_2 shell had the main catalytic role in the mechanism of the reaction which was the activation of the carbonyl groups of the β-diketone. Also, the doping agent (Sulfur atoms) had a synergistic effect on catalytic activity by increasing the electron density of the catalyst which resulted in higher surface adsorption of nanocatalyst.

In order to determine the relative configuration (syn or anti-diastereomer) of these newly synthesized tetrahydropyridines, the structure of compound **4g** was analyzed based on an extensive ^{1}H NMR experiment involving NOESY analysis. As shown in Fig. 6, the peaks correspond to the benzylic proton, and the methyl group on the six-membered ring of the tetrahydropyridine was investigated in the NOESY spectrum. The signal at $\delta = 1.22$ is assigned to the methyl group, and the singlet at $\delta = 3.42$ confirms the presence of a benzyl group. Absence of any points between benzylic H and CH_3 shows that they are exclusively trans and don't have any interactions with each other. However, NOESY effect can be seen between benzylic proton and the methylene group connected to acetyl which describes that these two groups are syn with each other. All the products were confirmed by spectroscopic methods using FTIR, ^{1}H NMR, ^{13}C NMR and mass spectrometry.

Fig. 5 Recyclability study of Fe_3O_4@S–TiO_2 for the model reaction

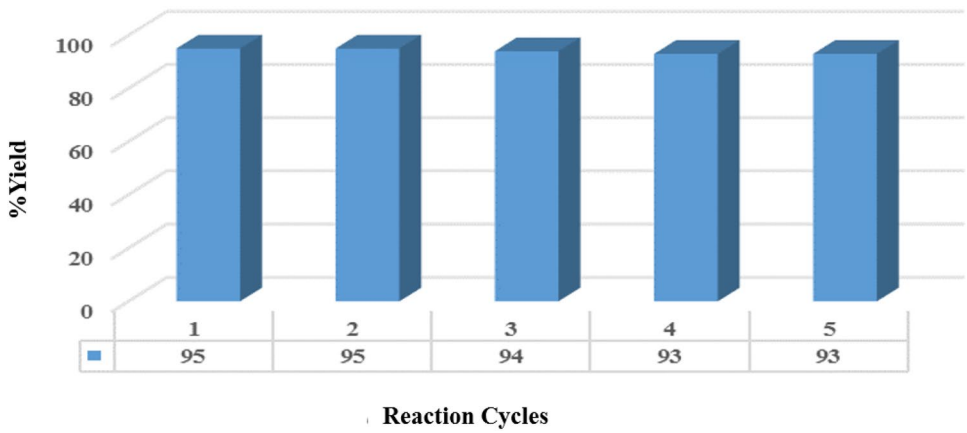

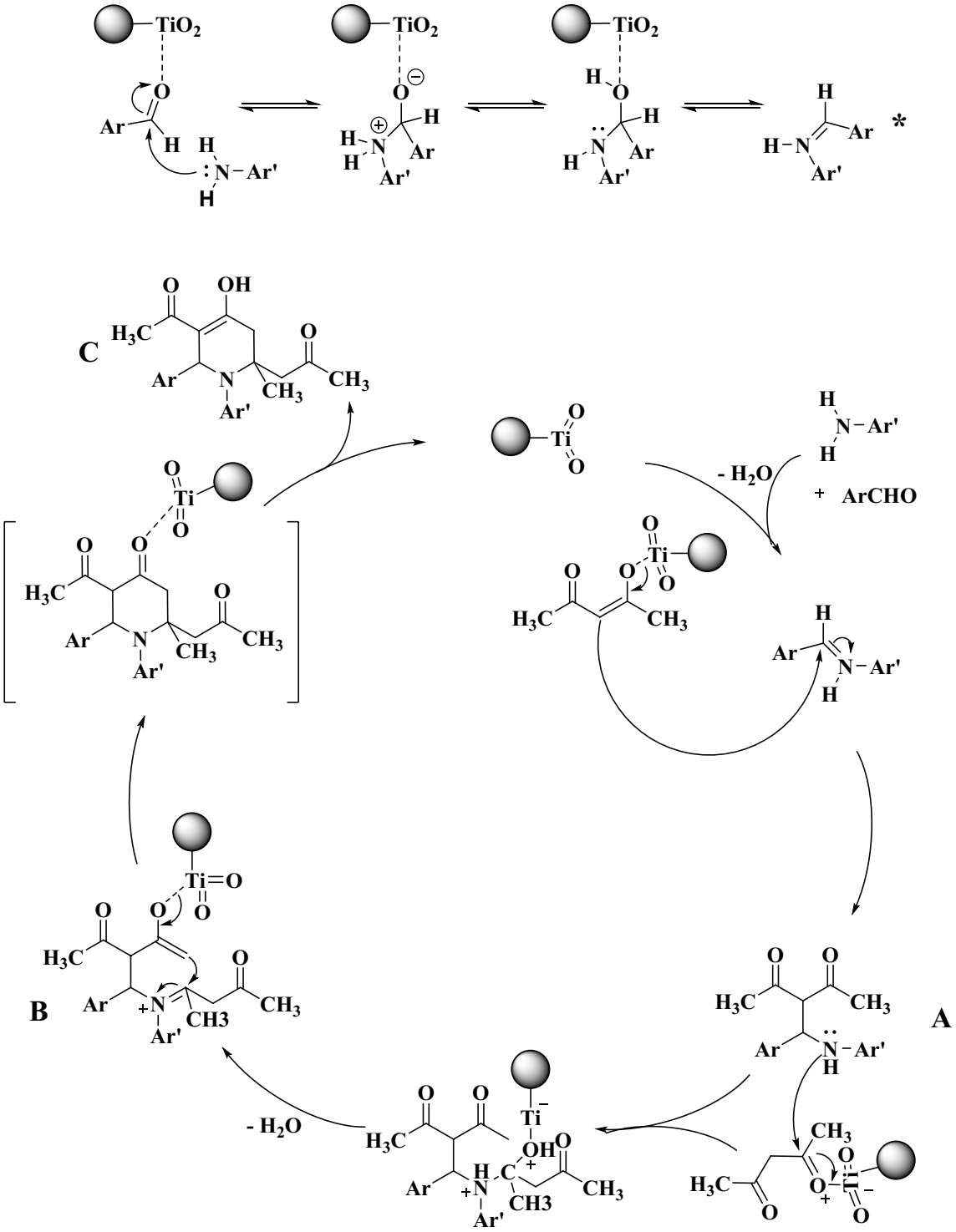

Scheme 3 Proposed mechanism for the reaction between substituted benzaldehydes, aniline derivatives and acetylacetone for making the tetrahydropyridine derivatives in the presence of Fe_3O_4@S–TiO_2

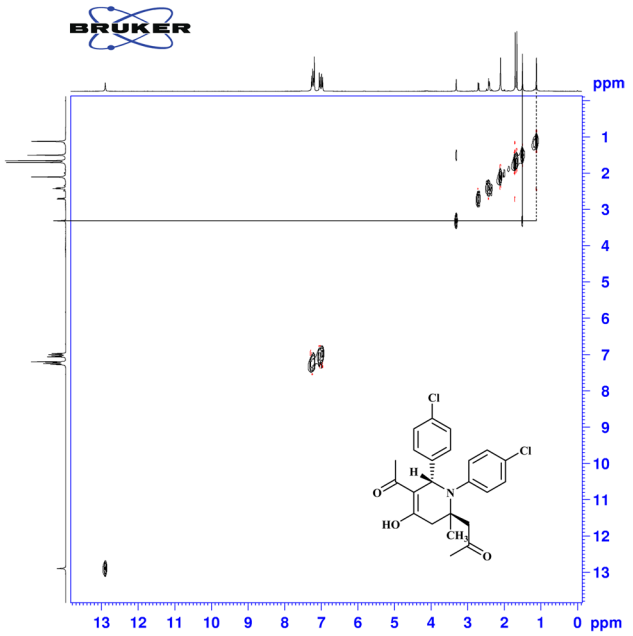

Fig. 6 H–H NOESY spectrum of 1-(5-acetyl-1,6-bis(4-chlorophenyl)-4-hydroxy-2-methyl-1,2,3,6-tetrahydropyridin-2-yl) propan-2-one (**4g**)

Conclusions

In summary, we have designed and prepared a magnetically recoverable green core–shell nanocatalyst that its shell was doped with sulfur atoms. The catalyst has been characterized by TEM, SEM, EDS, XRD, VSM and FTIR. After full characterization, these Fe_3O_4@S–TiO_2 NPs were used as a successful nanocatalyst for the synthesis of new highly substituted tetrahydropyridine derivatives. The desired reaction was the diastereoselective pseudo-four-component reaction of aromatic amines, aromatic aldehydes and acetylacetone at 100 °C and under solvent-free conditions. The Fe_3O_4@S–TiO_2 NPs after easy separation from the reaction mixture reused five times with high product yields. Besides, catalytic efficiency in comparison to the undoped the Fe_3O_4@TiO_2 NPs and its important role in the rate of the reaction was approved.

Experimental

General

All reagents and solvents were purchased from Merck and Fluka and used as received without further purification. The particle size and morphology of synthesized catalyst were characterized with a transmission electron microscope (TEM) (JEOL: JEM-1400 and Leo 912 AB) and field emission scanning electron microscope (FESEM) (TESCAN) equipped with EDX detector. The phase purity of the product was examined by X-ray diffraction (XRD) using a Bruker-D8 Advance X-ray diffractometer with Cu Kα radiation ($\lambda = 1.5406$ Å). Magnetic measurements for the nanoparticles were performed using a vibrating sample magnetometer (VSM, VSMF). Fourier transform infrared (FTIR) spectra were recorded on a Thermo Nicolet AVATAR-370 FTIR spectrophotometer using a KBr wafer. Melting points were measured on an Electrothermal type 9100 melting point apparatus. ^{1}H-NMR and ^{13}C-NMR spectra were measured ($CDCl_3$) with a Bruker DRX-300 AVANCE spectrometer at 300 and 75 MHz, respectively.

Preparation of magnetite hollow spheres (Fe_3O_4)

$FeCl_3 \cdot 6H_2O$ (1.35 g, 5.00 mmol) was dissolved in ethylene glycol (EG) (30 ml). After forming a clear solution, ethylenediamine (EDA) (3.00 ml) was added to the reaction mixture. The mixture was stirred vigorously until it became homogeneous, and then the resulting black solution was sealed in a Teflon-lined stainless-steel autoclave. The autoclave was heated at 200 °C for 12 h, and then naturally cooled to room temperature. The solid product was separated by using an external magnetic field and sequentially rinsed with distilled water and ethanol several times and then dried in an oven at 50 °C for 6 h.

Preparation of nanomagnetic sulfur-doped titanium dioxide (Fe_3O_4@S–TiO_2)

The obtained Fe_3O_4 powder (1.02 g, 4.40 mmol) was dispersed in 30 ml absolute ethanol by sonication for 10 min, and then Titanium (IV) isopropoxide (0.8 ml, 2.70 mmol) was added to the mixture. After magnetic stirring at room temperature, 5.6 ml thiourea/deionized water (volume ratio, 1:3) solution was added dropwise to the reaction mixture. After 60 min of stirring, the resulted suspension was transferred into a Teflon-lined stainless-steel autoclave, followed by heat treatment at 100 °C for 48 h. After cooling to room temperature, the catalyst was separated and washed with distilled water and ethanol for six times with the assistance of a magnet. Finally, the purified nanosphere of Fe_3O_4@S–TiO_2 was dried in an oven at 50 °C overnight.

Synthesis of tetrahydropyridine derivatives

A mixture of aromatic amines (1.0 mmol) and aromatic aldehydes (1.0 mmol) was stirred for 15–20 min to produce imine. Then acetyl acetone (2.0 mmol) and Fe_3O_4@S–TiO_2 (0.01 g) were added to the reaction mixture and refluxed for 4–6.5 h at 100 °C under solvent-free conditions. Upon completion, it was cooled to room temperature and then, the hot acetone was added to the reaction mixture to dissolve

the product, and the Fe_3O_4@S–TiO_2 was separated from the reaction mixture by employing an external magnetic field. Then, the reaction mixture was decanted to another vessel, and the catalyst thoroughly washed and dried to be reused in the next run. To another vessel, the solvent was evaporated, and the resulting crude product was purified with thin layer chromatography (*n*-hexane/ethyl acetate, 10:6). The spectral data for the products are described below.

1-(5-Acetyl-4-hydroxy-2-methyl-1,6-diphenyl-1,2,3,6-tetrahydropyridin-2-yl)propan-2-one (4a)

Yield = 88%. m.p. 89–90 °C. IR (KBr, cm^{-1}): ν 3396 (OH), 1712 (CO), 1657 (CO). ^{1}H-NMR ($CDCl_3$, 300 MHz, δ, ppm): 1.44 (s, 3H, CH_3), 1.78 (d, 1H, J = 7.2 Hz, C=CCH_2), 1.85 (d, 1H, J = 7.8 Hz, C=CCH_2), 2.03 (s, 3H, CH_3COCH_2), 2.12 (s, 3H, CH_3COC=C), 2.41 (d, 1H, J = 6.6 Hz, COCH_2), 2.68 (d, 1H, J = 6.6 Hz, COCH_2), 5.15 (s, 1H, CH_{Benzyl}), 7.03–7.13 (m, 3H, Ar–H), 7.29–7.43 (m, 7H, Ar–H), 13.04 (s, 1H, OH). ^{13}C-NMR ($CDCl_3$, 75 MHz, δ, ppm): 24.1, 27.8, 29.9, 45.7, 51.2, 53.1, 55.4, 104.2, 114.4, 120.7, 127.0, 128.5, 128.8, 129.3, 137.9, 150.1, 179.7, 196.6, 206.3. MS (*m/z*): 363. Elemental analysis for $C_{23}H_{25}NO_3$ (%): C, 76.01; H, 6.93; N, 3.85. Found: C, 76.20; H, 6.70; N, 3.69.

1-(5-Acetyl-6-(4-chlorophenyl)-4-hydroxy-2-methyl-1-phenyl-1,2,3,6-tetrahydropyridin-2-yl)propan-2-one (4b)

Yield = 86%. m.p. 236–238 °C. IR (KBr, cm^{-1}): ν 3339 (OH), 1711 (CO). ^{1}H-NMR ($CDCl_3$, 300 MHz, δ, ppm): 1.45 (s, 3H, CH_3), 1.64 (ABq, 2H, C=CCH_2), 2.14 (s, 6H, CH_3), 2.30 (d, 1H, J = 7.5 Hz, COCH_2), 2.56 (d, 1H, J = 7.5 Hz, COCH_2), 5.14 (s, 1H, CH_{Benzyl}), 7.03 (t, 1H, J = 3.9 Hz, Ar–H), 7.29 (d, 2H, J = 3.9 Hz, Ar–H), 7.45–7.50 (m, 6H, Ar–H), 13.08 (s, 1H, OH). ^{13}C-NMR ($CDCl_3$, 75 MHz, δ, ppm): 19.3, 19.3, 30.4, 30.4, 43.7, 50.9, 53.1, 59.8, 115.1, 121.7, 128.4, 128.6, 129.0, 129.6, 130.0, 132.2, 139.7, 143.7, 146.7, 146.8, 179.4, 198.7, 206.3. MS (*m/z*): 397. Elemental analysis for $C_{23}H_{24}ClNO_3$ (%): C, 69.43; H, 6.08; N, 3.52. Found: C, 69.92; H, 5.82; N, 3.51.

1-(5-Acetyl-4-hydroxy-2-methyl-6-(3-nitrophenyl)-1-phenyl-1,2,3,6-tetrahydropyridin-2-yl)propan-2-one (4c)

Yield = 90%. m.p. 87–88 °C. IR (KBr, cm^{-1}): ν 3328 (OH), 1528 (NO_2), 1348 (NO_2). ^{1}H-NMR ($CDCl_3$, 300 MHz, δ, ppm): 1.44 (s, 3H, CH_3), 1.84 (ABq, 2H, C=CCH_2), 2.07 (s, 3H, CH_3COCH_2), 2.37 (s, 3H, CH_3COC=C), 2.60 (d, 1H, J = 6.6 Hz, COCH_2), 2.73 (d, 1H, J = 6.9 Hz, COCH_2), 5.25 (s, 1H, CH_{Benzyl}), 6.83 (t, 1H, J = 6.6 Hz, Ar–H), 6.96 (d, 2H, J = 6.6 Hz, Ar–H), 7.12–7.43 (m, 4H, Ar–H), 8.06–8.26 (m, 2H, Ar–H), 13.17 (s, 1H, OH). ^{13}C-NMR ($CDCl_3$, 75 MHz, δ, ppm): 23.8, 26.9, 30.1, 45.3, 51.2, 53.2, 55.8, 105.1, 112.3, 121.9, 122.1, 129.3, 129.5, 134.0, 139.5, 147.7, 150.1, 178.8, 196.1, 206.4. MS (*m/z*): 408. Elemental analysis for $C_{23}H_{24}N_2O_5$ (%): C, 67.63; H, 5.92; N, 6.86. Found: C, 67.47; H, 6.13; N, 6.92.

1-(5-Acetyl-4-hydroxy-2-methyl-6-(4-nitrophenyl)-1-phenyl-1,2,3,6-tetrahydropyridin-2-yl)propan-2-one (4d)

Yield = 95%. m.p. 243–245 °C. IR (KBr, cm^{-1}): ν 3362 (OH), 1512 (NO_2), 1345 (NO_2). ^{1}H-NMR ($CDCl_3$, 300 MHz, δ, ppm): 1.77 (d, 1H, J = 6.3 Hz, C=CCH_2), 1.81 (d, 1H, J = 6.3 Hz, C=CCH_2), 2.06 (s, 3H, CH_3), 2.36 (s, 6H, CH_3), 2.87 (d, 1H, J = 6.6 Hz, COCH_2), 3.10 (d, 1H, J = 6.6 Hz, COCH_2), 5.21 (s, 1H, CH_{Benzyl}), 7.16–7.39 (m, 5H, Ar–H), 7.54 (d, 2H, J = 8.1 Hz, Ar–H), 8.24 (d, 2H, J = 8.1 Hz, Ar–H), 13.16 (s, 1H, OH). ^{13}C-NMR ($CDCl_3$, 75 MHz, δ, ppm): 25.80, 27.1, 30.1, 46.3, 51.2, 53.1, 58.4, 105.1, 110.5, 119.6, 123.5, 128.1, 130.0, 142.5, 146.2, 148.6, 178.1, 196.1, 206.6. MS (*m/z*): 408. Elemental analysis for $C_{23}H_{24}N_2O_5$ (%): C, 67.63; H, 5.92; N, 6.86. Found: C, 67.53; H, 6.06; N, 6.90.

1-(5-Acetyl-4-hydroxy-2-methyl-6-(4-phenylcyanide)-1-phenyl-1,2,3,6-tetrahydropyridin-2-yl)propan-2-one (4e)

Yield = 71%. m.p. 88–90 °C. IR (KBr, cm^{-1}): ν 3378 (OH), 2224 (CN). ^{1}H-NMR ($CDCl_3$, 300 MHz, δ, ppm): 1.65 (s, 3H, CH_3), 1.88 (d, 1H, J = 7.5 Hz, C=CCH_2), 1.91 (d, 1H, J = 7.5 Hz, C=CCH_2), 2.10 (s, 3H, CH_3COCH_2), 2.21 (s, 3H, CH_3COC=C), 2.47 (d, 1H, J = 7.8 Hz, COCH_2), 2.61 (d, 1H, J = 7.8 Hz, COCH_2), 4.61 (s, 1H, CH_{Benzyl}), 6.80–6.89 (m, 3H, Ar–H), 7.09 (t, 2H, J = 8.1 Hz, Ar–H), 7.46 (d, 2H, J = 8.1 Hz, Ar–H), 7.72 (d, 2H, J = 8.1 Hz, Ar–H), 12.81 (s, 1H, OH). ^{13}C-NMR ($CDCl_3$, 75 MHz, δ, ppm): 23.8, 28.5, 30.1, 45.0, 51.2, 53.2, 56.6, 104.4, 110.8, 114.3, 118.6, 122.0, 128.4, 129.5, 132.1, 142.6, 150.7, 179.8, 196.9, 206.1. MS (*m/z*): 388. Elemental analysis for $C_{24}H_{24}N_2O_3$ (%): C, 74.21; H, 6.23; N, 7.21. Found: C, 74.38; H, 6.01; N, 7.06.

1-(5-Acetyl-6-(2,4-dichlorophenyl)-4-hydroxy-2-methyl-1-phenyl-1,2,3,6-tetrahydropyridin-2-yl)propan-2-one (4f)

Yield = 90%. m.p. 226–228 °C. IR (KBr, cm^{-1}): ν 3417 (OH), 1588 (C=C). ^{1}H-NMR ($CDCl_3$, 300 MHz, δ, ppm): 1.54 (s, 3H, CH_3), 1.71 (d, 1H, J = 6.6 Hz, C=CCH_2), 1.78 (d, 1H, J = 6.3 Hz, C=CCH_2), 1.94 (s, 6H, CH_3), 2.51 (d, 1H, J = 8.7 Hz, COCH_2), 2.87 (d, 1H, J = 8.7 Hz, COCH_2), 4.56 (s, 1H, CH_{Benzyl}), 6.78–6.94 (m, 4H, Ar–H),

7.09–7.32 (m, 3H, Ar–H), 7.71 (s, 1H, Ar–H), 13.13 (s, 1H, OH). ^{13}C-NMR ($CDCl_3$, 75 MHz, δ, ppm): 23.6, 27.1, 29.8, 45.8, 50.6, 51.3, 53.7, 104.5, 113.9, 121.7, 126.8, 129.6, 130.3, 130.8, 134.0, 134.6, 135.3, 149.8, 179.6, 196.5, 206.8. MS (*m/z*): 431. Elemental analysis for $C_{23}H_{23}Cl_2NO_3$ (%): C, 63.90; H, 5.36; N, 3.24. Found: C, 63.87; H, 5.29; N, 3.53.

1-(5-Acetyl-1,6-bis(4-chlorophenyl)-4-hydroxy-2-methyl-1,2,3,6-tetrahydropyridin-2-yl)propan-2-one (4g)

Yield = 95%. m.p. 238–240 °C. IR (KBr, cm^{-1}): ν 3405 (OH), 1701 (CO). ^{1}H-NMR ($CDCl_3$, 300 MHz, δ, ppm): 1.22 (s, 3H, CH_3), 1.63 (d, 1H, J = 8.1 Hz), 1.75 (s, 3H, $C\underline{H}_3COCH_2$), 1.80 (s, 3H, $CH_3COC{=}C$), 2.52 (ABq, 2H, $C{=}CCH_2$), 2.81(d, 1H, J = 8.1 Hz), 3.42 (s, 1H, CH_{Benzyl}), 7.08 (d, 2H, J = 8.4 Hz, Ar–H), 7.14 (d, 2H, J = 8.4 Hz, Ar–H), 7.30–7.37 (m, 4H, Ar–H), 13.01 (s, 1H, OH). ^{13}C-NMR ($CDCl_3$, 75 MHz, δ, ppm): 28.1, 29.7, 34.9, 40.6, 45.0, 63.4, 68.7, 105.7, 127.1, 129.0, 129.3, 131.2, 132.5, 137.2, 144.2, 154.8, 179.8, 198.4, 215.9. MS (*m/z*): 431. Elemental analysis for $C_{23}H_{23}Cl_2NO_3$ (%): C, 63.90; H, 5.36; N, 3.24. Found: C, 63.90; H, 5.32; N, 3.62.

1-(5-Acetyl-1-(4-chlorophenyl)-4-hydroxy-2-methyl-6-(4-nitrophenyl)-1,2,3,6-tetrahydropyridin-2-yl) propan-2-one (4h)

Yield = 82%. m.p. 84–85 °C. IR (KBr, cm^{-1}): ν 3428 (OH), 1592 (NO_2), 1383 (NO_2), 1109 (CN). ^{1}H-NMR ($CDCl_3$, 300 MHz, δ, ppm): 1.38 (s, 3H, CH_3), 1.76 (ABq, 2H, $C{=}CCH_2$), 1.99 (s, 3H, $C\underline{H}_3COCH_2$), 2.20 (s, 3H, $CH_3COC{=}C$), 2.64 (d, 1H, J = 7.5 Hz, $COCH_2$), 2.88 (d, 1H, J = 7.8 Hz, $COCH_2$), 4.44 (s, 1H, CH_{Benzyl}), 6.61 (d, 2H, J = 7.8 Hz, Ar–H), 7.05 (d, 2H, J = 8.4 Hz, Ar–H), 7.52 (d, 2H, J = 8.4 Hz, Ar–H), 8.16 (d, 2H, J = 8.7 Hz, Ar–H), 12.91 (s, 1H, OH). ^{13}C-NMR ($CDCl_3$, 75 MHz, δ, ppm): 24.3, 27.3, 31.0, 45.5, 50.8, 53.4, 56.4, 104.9, 115.5, 125.8, 127.2, 128.3, 128.9, 143.2, 146.2, 147.8, 179.8, 197.1, 206.2. MS (*m/z*, %): 440 (5), 425 (12), 396 (8), 379 (12), 344 (23), 263 (13), 250 (4), 192 (16), 179 (8), 122 (10), 98 (17), 77 (33), 63 (10), 43 (100), 29 (9). Elemental analysis for $C_{23}H_{23}ClN_2O_5$ (%): C, 62.37; H, 5.23; N, 6.33. Found: C, 62.21; H, 5.44; N, 6.39.

1-(5-Acetyl-4-hydroxy-1-(4-methoxyphenyl)-2-methyl-6-(4-nitrophenyl)-1,2,3,6-tetrahydropyridin-2-yl) propan-2-one (4i)

Yield = 79%. m.p. 213–215 °C. IR (KBr, cm^{-1}): ν 3397 (OH), 1612 (CO), 1511 (NO_2), 1345 (NO_2), 1249 (COC). ^{1}H-NMR ($CDCl_3$, 300 MHz, δ, ppm): 1.58 (s, 3H, CH_3), 1.80 (d, 1H, J = 8.4 Hz, $C{=}CCH_2$), 1.84 (d, 1H, J = 8.4 Hz, $C{=}CCH_2$), 2.06 (s, 3H, $C\underline{H}_3COCH_2$), 2.35 (s, 3H, $CH_3COC{=}C$), 2.48 (d, 1H, J = 8.7 Hz, $COCH_2$), 2.60 (d, 1H, J = 8.7 Hz, $COCH_2$), 3.86 (s, 3H, OCH_3), 5.29 (s, 1H, CH_{Benzyl}), 6.90–6.97 (m, 4H, Ar–H), 7.53 (d, 2H, J = 8.7 Hz, Ar–H), 8.19 (d, 2H, J = 8.7 Hz, Ar–H), 13.19 (s, 1H, OH). ^{13}C-NMR ($CDCl_3$, 75 MHz, δ, ppm): 23.7, 27.0, 29.7, 45.8, 50.9, 53.1, 55.8, 56.9, 104.4, 115.1, 115.2, 127.3, 127.9, 140.3, 144.2, 146.2, 152.7, 179.0, 196.3, 206.5. MS (*m/z*, %): 421 (13), 419 (30), 375 (100), 359 (36), 327 (55), 295 (84), 238 (35), 210 (29), 148 (52), 92 (28), 77 (45), 57 (68), 43 (98), 30 (67). Elemental analysis for $C_{24}H_{26}N_2O_6$ (%): C, 65.74; H, 5.98; N, 6.39. Found: C, 65.62; H, 6.12; N, 6.43.

1-(5-Acetyl-4-hydroxy-1-(4-methoxyphenyl)-2-methyl-6-(4-phenylcyanide)-1,2,3,6-tetrahydropyridin-2-yl) propan-2-one (4j) Yield = 78%. m.p. 88–90 °C. IR (KBr, cm^{-1}): ν 3397 (OH), 2254 (CN), 1596 (C=C), 1249 (COC). ^{1}H-NMR ($CDCl_3$, 300 MHz, δ, ppm): 1.66 (s, 3H, CH_3), 1.90 (d, 1H, J = 6.9 Hz, $C{=}CCH_2$), 2.08 (s, 3H, $C\underline{H}_3COCH_2$), 2.21 (s, 3H, $CH_3COC{=}C$), 2.32 (d, 1H, J = 6.9 Hz, $C{=}CCH_2$), 2.50 (d, 1H, J = 8.4 Hz, $COCH_2$), 2.57 (d, 1H, J = 8.1 Hz, $COCH_2$), 3.80 (s, 3H, OCH_3), 4.60 (s, 1H, CH_{Benzyl}), 6.85 (d, 2H, J = 8.4 Hz, Ar–H), 7.16 (d, 2H, J = 8.4 Hz, Ar–H), 7.31 (d, 2H, J = 8.4 Hz, Ar–H), 7.49 (d, 2H, J = 8.4 Hz, Ar–H), 12.80 (s, 1H, OH). ^{13}C-NMR ($CDCl_3$, 75 MHz, δ, ppm): 23.8, 27.4, 30.1, 45.9, 50.6, 53.5, 55.5, 55.8, 104.2, 111.5, 114.8, 115.0, 118.1, 128.3, 132.4, 141.7, 142.1, 152.8, 178.6, 196.6, 206.1. MS (*m/z*): 418. Elemental analysis for $C_{25}H_{26}N_2O_4$ (%): C, 71.75; H, 6.26; N, 6.69. Found: C, 71.92; H, 6.04; N, 6.54.

References

1. Z. Ma, F. Zaera, in *Encyclopedia of Inorganic and Bioinorganic Chemistry*. ed. by R.A. Scott (Wiley, London, 2011)
2. L.M. Rossi, N.J.S. Costa, F.P. Silva, R. Wojcieszak, Green Chem. **16**, 2906 (2014)
3. L.H. Reddy, J.L. Arias, J. Nicolas, P. Couvreur, Chem. Rev. **112**, 5818 (2012)
4. N. Zhu, H. Ji, P. Yu, J. Niu, M.U. Farooq, M.W. Akram, I.O. Udego, H. Li, X. Niu, Nanomaterials **8**, 810 (2018)
5. S.N. Sun, C. Wei, Z.Z. Zhu, Y.L. Hou, S.S. Venkatraman, Z.C. Xu, *Chin. Phys. B* **23** (2014)
6. M. Stefan, O. Pana, C. Leostean, C. Bele, D. Silipas, M. Senila, E. Gautron, J. Appl. Phys. **116**, 114312 (2014)
7. A.K.P.D. Savio, J. Fletcher, F.C. Robles Hernandez, *Ceram. Int.* **39**, 2753 (2013)
8. C. Leostean, M. Stefan, O. Pana, A.I. Cadis, R.C. Suciu, T.D. Silipas, E. Gautron, J. Alloys Compd. **575**, 29 (2013)
9. C. Yang, H. Yan, Mater. Lett. **73**, 129 (2012)
10. A. Fujishimaa, X. Zhang, D.A. Tryk, Surf. Sci. Rep. **63**, 515 (2008)
11. T. Ohno, T. Mitsui, M. Matsumura, Chem. Lett. **32**, 364 (2003)
12. T. Ohno, M. Akiyoshi, T. Umebayashi, K. Asai, T. Mitsui, M. Matsumura, Appl. Catal. A **265**, 115 (2004)

13. T. Umebayashi, T. Yamaki, H. Itoh, K. Asai, Appl. Phys. Lett. **81**, 454 (2002)
14. L. Szatmáry, S. Bakardjieva, J. Šubrt, P. Bezdička, J. Jirkovský, Z. Bastl, V. Brezová, M. Korenko, Catal. Today **161**, 23 (2011)
15. L.G. Devi, R. Kavitha, Mater. Chem. Phys. **143**, 1300 (2014)
16. A. Khazaei, A.R. Moosavi-Zare, F. Gholami, V. Khakyzadeh, Appl. Organometal. Chem. **30**, 691 (2016)
17. A. Khazaei, M.A. Zolfigol, A.R. Moosavi-Zare, F. Abi, A. Zare, H. Kaveh, V. Khakyzadeh, M. Kazem-Rostami, A. Parhami, H. Torabi-Monfared, Tetrahedron **69**, 212 (2013)
18. M.A. Zolfigol, A. Khazaei, A.R. Moosavi-Zare, A. Zare, Z. Asgari, V. Khakyzadeh, A. Hasaninejad, J. Ind. Eng. Chem. **19**, 721 (2013)
19. A.R. Moosavi-Zare, M.A. Zolfigol, V. Khakyzadeh, C. Böttcher, M.H. Beyzavi, A. Zare, A. Hasaninejad, R. Luque, J. Mater. Chem. A **2**, 770 (2014)
20. A.R. Moosavi-Zare, M.A. Zolfigol, E. Noroozizadeh, M. Tavasoli, V. Khakyzadeh, A. Zare, New J. Chem. **37**, 4089 (2013)
21. M.A. Zolfigol, M. Tavasoli, A.R. Moosavi-Zare, P. Moosavi, H.G. Kruger, M. Shiri, V. Khakyzadeh, RSC Adv. **3**, 25681 (2013)
22. R.P. Gore, A.P. Rajput, Drug Invent. Today **5**, 148 (2013)
23. M. Srinivasan, S. Perumal, S. Selvaraju, Chem. Pharm. Bull. **54**, 795 (2006)
24. C. Ramalingan, Y.T. Park, S. Kabilan, Eur. J. Med. Chem. **41**, 683 (2006)
25. P. Chand, P.L. Kotian, A. Dehghani, Y. El-Kattan, T.H. Lin, T.L. Hutchison, Y.S. Babu, S. Bantia, A.J. Elliott, J.A. Montgomery, J. Med. Chem. **44**, 4379 (2001)
26. S. Petit, J.P. Nallet, M. Guillard, J. Dreux, R. Chermat, M. Poncelet, C. Bulach, P. Simon, C. Fontaine, M. Barthelmebs, J.L. Imbs, Eur. J. Med. Chem. **26**, 19 (1991)
27. Y. Zhou, V.E. Gregor, B.K. Ayida, G.C. Winters, Z. Sun, D. Murphy, G. Haley, D. Bailey, J.M. Froelich, S. Fish, S.E. Webber, T. Hermann, D. Wall, Bioorg. Med. Chem. Lett. **17**, 1206 (2007)
28. R. Aeluri, M. Alla, V.R. Bommena, R. Murthy, N. Jain, Asian. J. Org. Chem. **1**, 71 (2012)
29. S.A. Khanum, V. Girish, S.S. Suparshwa, N.F. Khanum, Bioorg. Med. Chem. Lett. **19**, 1887 (2009)
30. P.A. Clarke, A.V. Zaytzev, A.C. Whitwood, Tetrahedron Lett. **48**, 5209 (2007)
31. M. Misra, S.K. Pandey, V.P. Pandey, J. Pandey, R. Tripathi, R.P. Tripathi, Bioorg. Med. Chem. **17**, 625 (2009)
32. H. Wang, L. Mo, Z. Zhang, A.C.S. Comb, Sci. **13**, 181 (2010)
33. G. Brahmachari, S. Das, Tetrahedron Lett. **53**, 1479 (2012)
34. S. Mishra, R. Ghosh, Tetrahedron Lett. **52**, 2857 (2011)
35. S.S. Sajadikhah, N. Hazeri, M.T. Maghsoodlou, S.M. Habibi-Khorassani, A. Beigbabaei, A.C. Willis, J. Iran. Chem. Soc. **10**, 863 (2013)
36. W. Wu, X. Xiao, S. Zhang, F. Ren, C. Jiang, Nanoscale Res. Lett. **6**, 533 (2011)
37. S. Xuan, W. Jiang, X. Gong, Y. Hu, Z. Chen, J. Phys. Chem. C **113**, 553 (2009)
38. M. Abbas, B.P. Rao, V. Reddy, C. Kim, Ceram. Int. **40**, 11177 (2014)
39. M. Wu, H. Jing, T. Chang, Catal. Commun. **8**, 2217 (2007)

Affiliations

Zahra Nezami[1] · Hossein Eshghi[1]

✉ Hossein Eshghi
heshghi@um.ac.ir

[1] Department of Chemistry, Faculty of Science, Ferdowsi University of Mashhad, Mashhad, Iran